Exchange Rates of Surfactant at the Solid−Liquid Interface Obtained by ATR-FTIR

Spencer C. Clark and William A. Ducker*

Department of Chemistry, Virginia Tech, Blacksburg, Virginia 24061-0212

Received: February 10, 2003; In Final Form: June 3, 2003

There is at present considerable variance in the rates of surfactant adsorption and desorption that are reported in the literature. We have used in situ ATR−IR to measure the rate of adsorption, desorption and exchange of tetradecyltrimethylammonium bromide (C_{14}TABr) at the interface between silica and D_2O solutions. The rate of exchange was monitored by exposing an adsorbed layer of C_{14}TABr to a C_{14}TABr-d_{38} solution, while simultaneously monitoring the adsorption of both C_{14}TABr and C_{14}TABr-d_{38}. We find that the exchange of monomers between the surface and the bulk is very fast. Complete exchange occurs within about 10 s, even when exchange at the surface is limited by transport to the surface. A simple model for exchange suggests that the desorption rate for a single monomer is greater than 1 s^{-1}, which is no more than 10^4 times slower than for the desorption of a monomer from a micelle in bulk solution. Above and way below the cmc, the rate of adsorption of surfactant (exchange with solvent or its dissociation products) is similarly rapid. The rate of desorption is rapid, but slow enough for us to discern a break in the desorption rate. The results are consistent with the transport-limited desorption of the surfactant that is held by hydrophobic association with other surfactant molecules, and activation limited desorption of the surfactant that is electrostatically held to the surface. The rates of adsorption, exchange, and desorption were almost the same when the experiment was performed 11 °C above and 8 °C below the Krafft temperature of the surfactant.

Introduction

In many cases, surfactant adsorption and desorption at solid−liquid interfaces is found to be quite slow considering that surfactants are small molecules.[1,2] Some workers report adsorption times of hours or even days before equilibrium is reached[2−4] whereas others report that equilibrium for surfactant adsorption is reached quickly, in only about 20 s.[5] Considering these results, surprisingly little attention has been directed to the measurement of fundamental kinetic parameters for surfactant exchange at interfaces. In contrast, the exchange of surfactant monomers between bulk micelles and solution has been well studied. Temperature-jump and pressure-jump experiments, combined with the theoretical interpretation of Aniansson et al.[6] have allowed quantitation of the on and off rates, k^+ and k^-, for surfactant association into micelles:

$$H_{S-1} + H \rightleftharpoons H_S \quad (1)$$

where H_S is a surfactant micelle of aggregation number, S.

Typical values of k^+ are close to diffusion limited, whereas k^- is activation limited. Because k^- is related to the probability of any one of many monomers leaving the micelle, values are often reported as k^-/n, where n is the aggregation number. For example, $k^-/n = 1.0 \times 10^4$ s^{-1} for tetradecyltrimethylammonium bromide (C_{14}TABr) at 25 °C.[7]

The same temperature-jump and pressure-jump experiments also reveal a slower process (τ_2), which has been assigned to the change in number of micelles after a change in pressure or temperature.

Thus, studies of surfactant adsorption and desorption kinetics imply that desorption from the solid−solution interface is much slower than the analogous processes in bulk solution. It is likely that some of the longer time constants are due either to the presence of impurities or to slow transport to the surface. If an experiment simply measures the rate of adsorption, it is important to note in the analysis that adsorption requires transport to or from the surface (by convection and diffusion) as well as processes that occur at the interface. For example, Couzis and Gulari showed that adsorption of sodium dodecyl sulfate to alumina was diffusion-limited in their apparatus.[8] Clearly, there is a big range of measured rates for adsorption and desorption, but all the literature seems to agree that the rates are much slower than in bulk: either the exchange of individual surfactant monomers at interfaces is quite slow, or desorption from surface aggregates involves passage through some very unfavorable aggregation numbers. In other words, the desorption process has another time constant analogous to the τ_2 sampled in *T*-jump and *p*-jump experiments, but much slower. Accordingly, the corresponding kinetic barriers at the surface would also be much larger than in bulk.

Atomic force microscopy (AFM) imaging studies also provide some indirect evidence on the longetivity of micelles. In AFM imaging, individual micelles *appear* to be stable for several fast-scan time constants (∼1 s) and perhaps for the duration of entire scans (∼1 min).[9,10]

When the exchange rates between surfactants associated at interfaces, and between surfactants in bulk, are comtemplated, a reasonable approach would seem to be to start with the known value for the k^+ ad k^- for bulk micelles, and then to consider the factors that would tend to slow desorption or adsorption of monomers. Clearly, exchange from the solid side of any adsorbed micelle will be hindered both by the presence of an overlying layer and by attractive interactions with the solid. Differences between rate constants for bulk micelles and rate constants for surfactants associated at interfaces should also arise

* Corresponding author. Tel: 540-231-2249. Fax: 540-231-3255. E-mail: wducker@vt.edu.

10.1021/jp034347a CCC: $25.00
Published on Web 07/30/2003

from differences in the structure of adsorbed micelles, differences in crystallization that are induced by the surface, changes induced by the proximity of neighboring micelles and, for charged surfactants, changes in activation energy caused by the electrical potential at the solid−liquid interface. The existence of anisotropy within the surface micelle naturally introduces an additional kinetic constant: the rate of exchange between different parts of adsorbed micelles.

In this paper, we investigate the adsorption and desorption kinetics of the cationic surfactant, tetradecyltrimethylammonium bromide (C_{14}TABr), to negatively charged silica through attenuated total reflectance Fourier transform infrared spectroscopy (ATR−FTIR). Adsorption from or desorption to solution is necessarily an exchange process where the surfactant is replaced by solvent or other solutes. Here our main focus is on exchange of one surfactant for another surfactant, but we also examine exchange for water (including its dissociation product, the proton) and for salt and water.

ATR−IR has previously been used to measure surfactant adsorption by several research groups.[3,11−18] The chief advantages of ATR−FTIR are that it enables one to monitor the adsorption of more than one species simultaneously, in situ, with a resolution of about 0.1−2 s. Most techniques that measure surface excess are either slower (e.g., neutron reflection) or cannot simultaneously and separately measure the adsorption of several species. For example, ellipsometry, reflectometry, and surface plasmon resonance have all been very useful in measuring surfactant adsorption, but because they monitor the refractive index, contributions from different adsorbates cannot be directly deconvoluted. In contrast, ATR−FTIR can be used to monitor the adsorption of several species providing that all but one of the IR chromophores absorb at different frequencies. FTIR can also provide information about the orientation of the molecules, through polarization studies,[14,19,20] and about intermolecular bonding, though the examination of frequency shifts.[3,21−24]

Here we make use of the fact that substitution of deuterium for hydrogen in a surfactant produces a large change in IR absorption frequencies, while causing relatively small changes in chemistry. We are able to examine the exchange of one surfactant for another by adsorbing a surface film of hydrogenated C_{14}TABr in equilibrium with C_{14}TABr solution, and then quickly replacing the solution with perdeuterated C_{14}TABr (C_{14}-TABr-d_{38}). Using ATR−FTIR we can monitor the desorption of C_{14}TABr and simultaneously the adsorption of C_{14}TABr-d_{38}. If we assume that the properties of a monomer in an adsorbed micelle are independent of whether its neighbors are C_{14}TABr or C_{14}TABr-d_{38} molecules, then the same monomer desorption process is being monitored throughout the surfactant exchange. In some ways our measurements are analogous to *T*-jump and *p*-jump experiments, except that the perturbation is in monomer concentration, and therefore our time resolution is often limited by solution exchange times and transport to the surface. Our experiments could therefore be described as a "concentration saunter".

An outline of the paper is as follows. We first describe the use of FTIR for measuring an adsorption isotherm and discover the interesting regimes for kinetics studies. Aggregation of C_{14}TABr on silica occurs below the critical micelle concentration (cmc), so we have monitored exchange at 0.07 cmc, 0.75 cmc, and 1.50 cmc. We then describe the kinetics of adsorption, exchange, and desorption for surfactant-only solutions at 25 °C, the impact of salt, and the exchange at ∼6 °C. Finally, we use AFM force measurements to obtain independent evidence for rearrangement times under a pressure induced by an AFM tip. All experiments used D_2O as the solvent instead of H_2O because there is an overlap of the H_2O peak with the protonated methyl stretch so the use of D_2O avoids the need to deconvolve overlapping spectral bands.

Experimental Section

Reagents. Tetradecyltrimethylammonium bromide (C_{14}TABr) from Sigma was recrystallized three times from acetone and a fourth time from absolute ethanol, which was vacuum distilled at room temperature. Perdeuterated tetradecyltrimethylammonium bromide (C_{14}TABr-d_{38}) (The Thomas Group, Oxford, U.K.) was used as received. According to the manufacturer, each molecule has 98% D and 2% H. From integration of the IR absorption in an ATR experiment, we find 97.5% D. Deuterium oxide (99.9%) was purchased from Cambridge Isotope Laboratories (U.K.) and distilled prior to use. Solutions were degassed (by placing the open D_2O container in a vacuum chamber and evacuating the chamber to ∼0.5 Torr for 3 to 5 min) and the pD was not altered with acids or bases, so the experimental results should be roughly comparable to those obtained in H_2O at pH 7. Degassing was performed to prevent bubble formation within the ATR flow cell during experiments. Potassium bromide from Aldrich was roasted at 300 °C in air ∼12 h to eliminate organic impurities.

Silica Substrate Preparation. The native oxide layer of a silicon internal reflection element (IRE) (Wilmad, Buena, NJ) was cleaned by rinsing in absolute ethanol and scrubbing lightly with a cotton-tipped applicator. The IRE was rinsed in distilled, deionized H_2O with a conductivity of 18.3 MΩ/cm at 25 °C prepared by an EASYpure UV system (model D7401, Barnstead Thermolyne Co., Dubuque, IA) and then dried in a stream of ultrapure nitrogen. The optical faces of the IRE were treated with UV radiation from an UVP Pen Ray lamp (UVP, Upland, CA) at a distance of ∼5 mm for 30 min. The IRE was sealed in the flow cell immediately following the UV treatment.

Atomic Force Microscope (AFM) Experiments. AFM force curves in C_{14}TABr/D_2O were measured using a Digital Instruments Nanoscope III AFM and a silicon nitride cantilever and tip with a nominal spring constant of 0.24 N m^{-1}. The range of the force curves was 300 nm.

FTIR−ATR Measurements. IR spectra were collected using a Nicolet Nexus 670 Fourier transform infrared spectrometer (Madison, WI) equipped with a liquid nitrogen cooled MCT-A detector, a Ge on KBr beam splitter, and a vertical variable-angle ATR accessory from CIC Photonics (Albuquerque, NM). The time required to capture a spectrum was about 2 s. Dry nitrogen was used as a purge gas. The custom silicon IRE, 80.0 × 8.0 × 3.20 mm, was a single pass 45° parallelogram crystal.

The IRE was sandwiched between two Teflon flow cells fitted with Kalrez 8201 O-rings. The cell design, shown in Figure 1, allows circulation of fluid across the full length of both optical faces, and solutions contact only glass, Teflon, the Kalrez O-rings and the IRE surface. The two solution cells had approximate dimensions of 0.5 mm thick × 7.5 mm wide × 78.5 mm long. Solutions were circulated using a peristaltic pump with a rigid PTFE-tubing pump head (Masterflex) and were isolated from the ambient atmosphere. The temperature of the flow cell was controlled, to minimize temperature-induced fluctuation of the OD stretch of D_2O at 2500 cm^{-1}. The temperature of the flow cell was controlled by circulating water through a copper heat sink cemented to the nonoptical faces of the IRE. The temperature of the surfactant solutions prior to entry to the cell was controlled by a heat exchanger at the cell entrance.

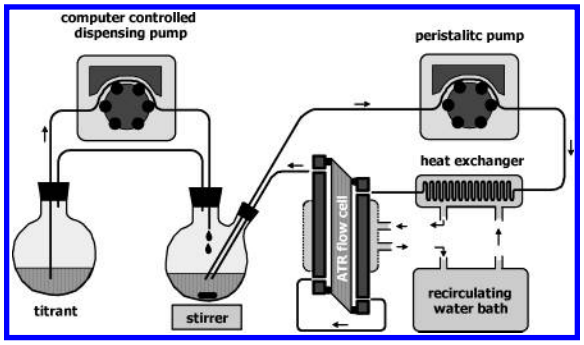

Figure 1. Experimental setup used for equilibrium experiments. Kinetic experiments utilized the same setup, but without the titration components.

To avoid contamination from oils and plasticizers, the Teflon flow cell and all other hardware that came in contact with surfactant solutions were cleaned before each experiment. Teflon tubing was washed with Liqui-Nox detergent solution, rinsed with ultrapure water and then blown dry with nitrogen. Glassware was washed with Liqui-Nox solution, rinsed in ultrapure water, soaked in hot base bath, rinsed in ultrapure water, and then dried in an oven at 150 °C. The flow cell, O-rings, and all fittings were sonicated in a solution of C_{12}TABr for 15 min, rinsed in ultrapure water, sonicated in ultrapure water for 15 min, and then blown dry with nitrogen. Cleaning and assembly were done while wearing gloves, and final assembly of the cell was done in a laminar flow cabinet. All experiments were performed at 25 ± 0.2 °C, except data shown in Figure 10, which is at 6.0 ± 0.3 °C. The temperature was controlled using a thermostated water bath (VWR) and measured at the outlet and inlet to the cell.

Transmission Molar Absorption Experiments. Molar absorption coefficients for the protonated and deuterated surfactants were determined using a transmission cell with a known path length of 104 μm. The C_{14}TABr molar absorption coefficient was measured in D_2O. The molar absorption coefficient of C_{14}TABr-d_{38} in D_2O was obtained by multiplying the absorption coefficient of C_{14}TABr by the ratio of C_{14}TABr-d_{38} absorption coefficient in methanol to the C_{14}TABr absorption coefficient in methanol-d_4.

Isotherm Experiment. Prior to an experiment, the detector was cooled to liquid nitrogen temperatures and the interferometer was aligned. The ATR flow cell was placed in the spectrometer bay and aligned. Background spectra were taken with no solution in the flow cell. The flow cell was then connected to the recirculating water bath (VWR) and the D_2O reservoir. Freshly distilled and degassed D_2O was pumped across the crystal surface at a rate of 2.0 mL/min. The interferometer and equipment were left running and allowed to equilibrate for 12 h before recording any measurements. Experiments were started after sample spectra of D_2O referenced to a D_2O background were linear, with minimal fluctuation in the D_2O stretching region. All sample spectra were 128 co-added scans collected in triplicate and referenced to pure D_2O. C_{14}TABr titrant was added to a recirculating C_{14}TABr solution. The surfactant concentration was stepped from zero to 7.0 mM in 22 intervals and allowed to equilibrate for 50 min before collecting sample spectra. Spectrometer settings used for isotherm experiments are as follows: mirror velocity 0.9494 cm/s, 2 cm^{-1} resolution, no zero filling, gain setting of 1.0, $-\log(R)$ format and Happ Genzel apodization.

Kinetic Experiments. The procedure was similar to that used in the isotherm experiments, except for a 3 h equilibration period, a mirror velocity of 1.2659 cm/s, and 4 cm^{-1} resolution. The procedure used to observe adsorption, exchange, and desorption of C_{14}TABr from the surface is as follows. Pure D_2O or KBr solutions were used to establish the initial baseline. The solution input was switched to C_{14}TABr solution, to C_{14}TABr-d_{38} solution, back to C_{14}TABr solution, and then to D_2O or KBr solution. A limiting factor in our kinetic resolution was the time for solution of the new concentration to diffuse though the low velocity (stagnant) layers near the optical surface. We succeeded in reducing this time by separating the old and new solutions with a small bubble (~0.25 mL). When the bubble passed through the cell, it spanned almost the entire width and thickness of the cell and, therefore, provided a more sudden change in solution concentration by exchanging solution very close to the optical surface. We could also monitor the passage of the bubble through the ATR cell using the FTIR spectrometer. For 0.07 cmc solutions, the bubble penetrated the evanescent zone, and the passage of the bubble could have altered the surface structure. For 1.5 cmc and 0.7 cmc, the bubble did not penetrate the evanescent zone ($3d_p \sim 700$ nm thick) and it was safe to assume that it provided a rapid flush without immediately disturbing the surface film. Experiments utilizing a bubble and those not utilizing a bubble are labeled "bubble" and "no-bubble", respectively. The pump flow rate was set at 7.5 mL/min for the initial 2 mL of solution and reduced to 2.0 mL/min thereafter.

Adsorption of C_{14}TABr. The initial C_{14}TABr solution was allowed to adsorb for 3 h. One-scan spectra were collected at 2.2 s intervals during the first minute of adsorption, 8-scan spectra were collected at six second intervals for the next 2.5 min and 256-scan spectra at 10 min intervals for a period of 200 min. Three 128-scan background spectra were taken after the equilibration period of 2.5 h with C_{14}TABr adsorbed to the SiO_2 surface.

Exchange from C_{14}TABr to C_{14}TABr-d_{38} to C_{14}TABr. After the initial adsorption of protonated surfactant, the solution was switched to deuterated surfactant at the same concentration. One scan spectra were collected at 2.2 s intervals for the first minute, and 8-scan spectra were collected at six second intervals for the next two minutes. Five 256-scan spectra were collected over a period of 16 min. The C_{14}TABr-d_{38} solution was switched back to C_{14}TABr and the same scan protocol was followed.

Desorption of C_{14}TABr. C_{14}TABr solution was switched to pure D_2O or to a solution of KBr in D_2O. Single scan spectra were collected at 2.2 s intervals for the first 2 min and 256-scan spectra were collected at 3.2 min intervals for another 32 min.

Theory

Surface Excess Determination. The infrared absorption by the surfactant depends on the electric field strength, which decays exponentially as a function of distance, z, from the interface between the reflection element and the solution. Because we do not know the z dependence of the surfactant concentration, we calculated the electric field strength at $z = 0$ for the entire surface excess. A typical decay length of the evanescent wave is 140 nm, so this approximation is less valid when concentration fluctuations extend to distances greater than ~50 nm. The Gibbs surface excess, Γ, of the surfactant at the interface between the silicon reflection element and the surfactant in D_2O solution was determined using the following expressions:[13,25−28]

$$-\log(R) = N\epsilon C_{\text{bulk}} b_{\text{eff}} + N\epsilon \frac{b_{\text{eff}}}{d}\Gamma \qquad (2a)$$

$$-\log(R) = N\epsilon \frac{b_{\text{eff}}}{d}\Gamma^* \tag{2b}$$

$-\log(R)$ is the integrated absorbance of the CH and CD stretching bands. The shape and position of the absorption peak depend on the environment of the surfactant so the use of absorption at a single frequency in eq 2 could introduce artifacts arising from changes in the surfactant environment. Therefore, we used the integrated absorbance of the entire peak. N is the number of internal reflections, ϵ is the transmission molar absorption coefficients of the surfactant, and C_{bulk} is the concentration of surfactant in bulk solution. Γ^*, which is defined by eq 2b, includes all contributions in the evanescent zone, and gives an approximate value of the surface excess.

The optical properties of the interface are modeled as a multilayer system, where the subscripts 1−3 refer respectively to the silicon reflection element, the immediately adsorbed adjacent layer, and the bulk solution. The penetration depth, d, is determined from the expression

$$d = \frac{\lambda}{4\pi \text{Im}(\xi_3)} \tag{3}$$

where λ is the infrared radiation wavelength and $\xi_{j=2,3} = [\hat{n}_j^2 - n_1^2 \sin^2(\theta)]^{1/2}$ is a function of the incident angle θ, the refractive index of the originating medium, n_1, and the complex refractive indices of medium two and three, $\hat{n}_{j=2,3}$. The complex refractive index is defined as $\hat{n}_j = n_j + ik_j$, where n_j is the real refractive index and k_j the absorption coefficient. The effective path lengths, b_{eff}, for each polarization were calculated using

$$b_{\text{eff,s}} = \frac{d\langle E_y^2\rangle n_3}{n_1 \cos(\theta)} \qquad b_{\text{eff,p}} = \frac{d\langle E_x^2\rangle n_3}{n_1 \cos(\theta)} + \frac{d\langle E_z^2\rangle n_3}{n_1 \cos(\theta)} \tag{4}$$

where s and p refer respectively to the electric field polarized perpendicular and parallel to the plane of incidence. The effective path length,[29] beff,unp, is dependent on the spectrometer polarization ratio[30] PR, which is unique to the instrument and experimentally determined.

$$b_{\text{eff,unp}} = \frac{\text{PR}\cdot b_{\text{eff,s}}}{\text{PR}+1} + \frac{b_{\text{eff,p}}}{\text{PR}+1} \tag{5}$$

The mean square electric amplitudes in phase $\hat{n}_3$ at the total internal reflection interface, $\langle E_x^2\rangle$, $\langle E_y^2\rangle$, and $\langle E_z^2\rangle$ are required to quantitate surfactant adsorption. Hansen has published the most comprehensive equations for determining mean square electric amplitudes for an evanescent wave as a function of distance from the interface and the complex refractive index of intermediate and final phases.[25,31−34]

$$\langle E_x^2\rangle = \left|\frac{t_p}{\hat{n}_3}\xi_3\right|^2 \exp\left(-\frac{(z-h)}{d}\right) \tag{6}$$

$$\langle E_y^2\rangle = |t_s|^2 \exp\left(-\frac{(z-h)}{d}\right) \tag{7}$$

$$\langle E_z^2\rangle = \left|\frac{t_p n_1 \sin(\theta)}{\hat{n}_3}\right|^2 \exp\left(-\frac{(z-h)}{d}\right) \tag{8}$$

The x and z directions lie in the plane of incidence with the z direction normal to the solid liquid interface. The y direction is perpendicular to the plane of incidence. The distance from the n_1, $\hat{n}_2$ interface is z, and the thickness of the second phase is h.

The Fresnel transmission coefficients t_p and t_s are

$$t_s = \frac{t_{s12}t_{s23}\exp(i\beta)}{1 + r_{s12}r_{s23}\exp(2i\beta)} \tag{9}$$

$$t_p = \frac{n_1 t_{p12}t_{p23}\exp(i\beta)}{\hat{n}_3[1 + r_{p12}r_{p23}\exp(2i\beta)]} \tag{10}$$

$t_{p,jk}$, $t_{s,jk}$, $r_{p,jk}$, and $r_{s,jk}$ are the Fresnel transmission and reflection coefficients for each planar phase boundary in the system

$$t_{s,jk} = \frac{2\xi_j}{\xi_j + \xi_k} \tag{11}$$

$$t_{p,jk} = \frac{2\hat{n}_k^2\xi_j}{\hat{n}_k^2\xi_j + \hat{n}_j^2\xi_k} \tag{12}$$

$$r_{s,jk} = \frac{\xi_j - \xi_k}{\xi_j + \xi_k} \tag{13}$$

$$r_{p,jk} = \frac{\hat{n}_k^2\xi_j - \hat{n}_j^2\xi_k}{\hat{n}_k^2\xi_j + \hat{n}_j^2\xi_k} \tag{14}$$

β is defined as $\beta = 2\pi\xi_3 h/\lambda$. ξ_1 is defined as $\xi_1 = n_1 \cos(\theta)$.

Analysis of ATR−IR Results

FTIR Spectra. All $-\log(R)$ spectra were collected without the use of a polarizer or optical filters. Figure 2 shows the adsorption spectra of C_{14}TABr and C_{14}TABr-d_{38}, and the

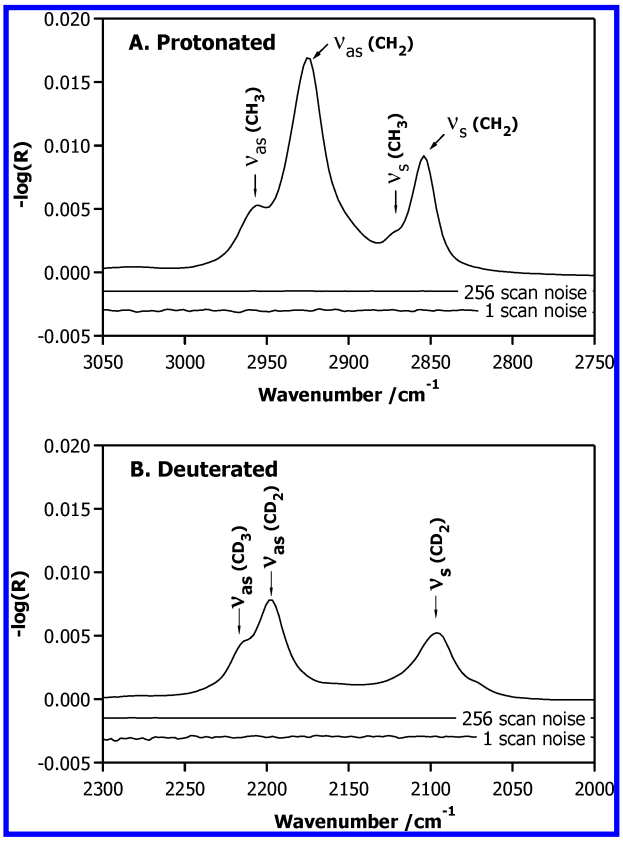

Figure 2. Sample spectra of (A) C_{14}TABr and (B) C_{14}TABr-d_{38}. Noise levels for a single scan and 256 scans are demonstrated by the two spectra beneath the stretch bands, which were measured in the absence of surfactant.

TABLE 1: Weighted-Average Wavenumber and Complex Refractive Indices for Protonated and Deuterated C_{14}TABr Absorption Bands

variable	C_{14}TABr	C_{14}TABr-d_{38}
$\bar{\nu}$	2910 cm^{-1}	2159 cm^{-1}
n_1	3.430 + 0.000i	3.425 + 0.000i
$\hat{n}_2 = \hat{n}_3$	1.236 + 0.002i	1.399 + 0.014i

assigned bands.[21,22] The distinct separation of the chromophores allows us to independently monitor the absorption of C_{14}TABr and C_{14}TABr-d_{38}.

Spectra from all experiments were linear baseline corrected, zeroed, and peak areas integrated using Mathcad (version 8.0 Professional, service pack 3). Protonated symmetric and asymmetric stretch bands were integrated from 2800 to 3000 cm^{-1}. Deuterated symmetric and asymmetric stretch bands were integrated from 2025 to 2265 cm^{-1}. To quantitate adsorbed C_{14}TABr-d_{38}, all spectra involving exchange of protonated and deuterated surfactant were referenced to a background spectrum taken after the initial adsorption of C_{14}TABr had reached equilibrium.

Calculation of Mean Square Electric Amplitudes. Weighted averages for the wavelength and complex refractive indices over the integration region for the protonated and deuterated C_{14}TABr absorption bands are given in Table 1.[35]

The incident angle as read from the ATR accessory was 60.0°, which corresponds to an internal incident angle of 49.3°. Due to the large fluctuation of surfactant at the surface in the kinetic experiments and considering the findings of Hair and Axelsen, we decided to treat the interface as a two layer system.[3,33] We set $\hat{n}_2 = \hat{n}_3$, so $h = 0$.[36] The mean square electric fields were calculated using Maple 7 (Waterloo Maple Inc., Onatrio, Canada).

Calculation of Gibbs Surface Excess. Gibbs surface excess values were calculated from integrated $-\log(R)$ values. The ATR incident angle was set experimentally to obtain 22.0 internal reflections. A method similar to that suggested by Sperline was used to verify that all 22 internal reflections sensed the solution.[37] Verification of the number of internal reflections utilized a solution of D_2O in H_2O and a transmission cell with a 100 μm path length. The Nicolet Nexus 670 FTIR spectrometer polarization ratio PR = 0.566 was determined using a wire grid polarizer (Molectron IGP-228, Location) with an efficiency of 97% at 3000 cm^{-1}.

Results and Discussion

Equilibrium Measurements. Figure 3 shows the adsorption isotherm for C_{14}TABr in D_2O at neutral pD. The isotherm is similar to one obtained by ellipsometry in H_2O at pH 9.7. The conditions and results are not identical, but the similarity between the two results supports the validity of using ATR−IR to detect adsorbed species. The break in the curve shows that the cmc of C_{14}TABr in D_2O is about 3.2 mM. The absence of a maximum in Γ near the cmc is consistent with the absence of surface active impurities in our system.

The frequency of the maximum in IR adsorption has been used as an indication of the environment of a chemical species.[21−23] A shift to lower frequency can be attributed to a smaller gradient in the bond force and has often been attributed to a more crystalline state and or to an increase in trans conformations in alkyl chains. Figure 4 shows the frequency of maximum adsorption of the CH_2 asymmetric stretch as a function of concentration. Here we are probably not sensing a change in crystallization, and we will merely use the frequency shift to indicate a qualitative change in the environment of the surfactant alkyl chain. In bulk solution, the frequency decreases above the cmc because of contributions arising from the different environment for molecules in the micelle compared to the environment of the monomer. The ATR frequency also decreases with concentration, which is consistent with aggregation at the surface (as described previously in ref 23). Note that the shift in frequency starts at a lower concentration at the surface than in bulk, consistent with the formation of aggregates on the surface in equilibrium with a monomeric solution in bulk.

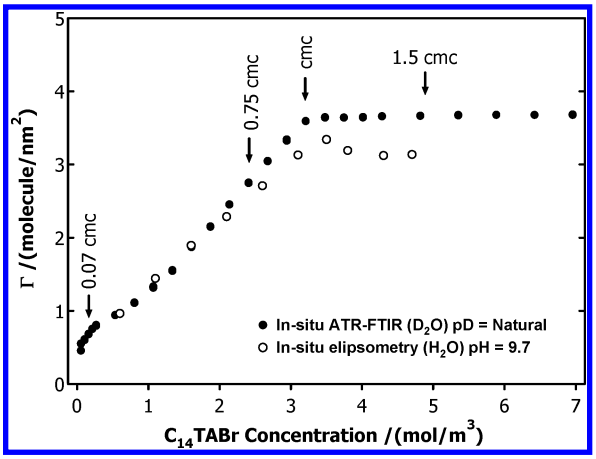

Figure 3. Asdorption isotherm of C_{14}TABr on the native SiO_2 surface of the silicon ATR element. In situ elipsometry data was taken from Wängnerud and Jönsson (*Langmuir* **1994**, *10*, 3268).

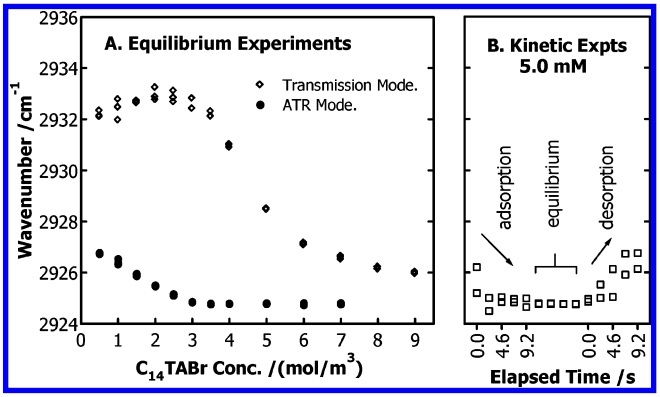

Figure 4. Peak maximum of CH_2 ν_{as} for C_{14}TABr. (A) At equilibrium: in transmission experiment (sensing surfactant in bulk) and ATR−FTIR experiment (sensing mainly adsorbed surfactant). (B) During kinetic experiments.

The remainder of the results describe nonequilibrium (kinetic) experiments. The shape of the adsorption isotherm, together with the frequency shift data suggest that the structure and environment on the surface varies according to the concentration, and therefore that we should investigate several concentration regimes. We have chosen to study the surface at 0.07 cmc, 0.75 cmc, and 1.5 cmc. Schematic and speculative figures of the adsorbed structures are shown in Figure 5. The 0.07 cmc is above the steep rise in Γ, so there is probably some interaction between alkyl tails of the adsorbed surfactant; at 0.75 cmc there are probably surface micelles, but no bulk micelles; and at 1.5 cmc there are bulk and surface micelles, with higher aggregation numbers for the surface micelles.[38]

Kinetic Experiments. Figure 6 shows a time series of spectra for a typical experiment. In this case the replacement of C_{14}TABr-d_{38} aggregates by C_{14}TABr is complete within 9 s. Spectra show that the quantity of water in the evanescent zone is constant during the exchange, and that after surface exchange occurs, the solution can be exchanged back to obtain the original

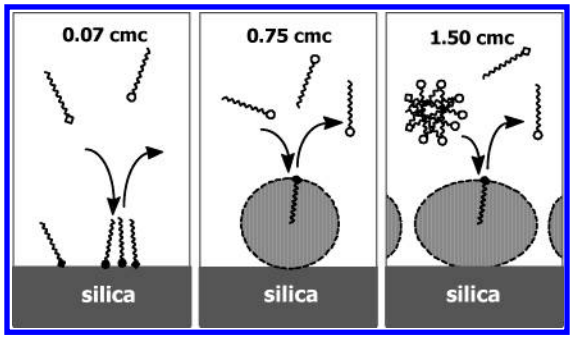

Figure 5. Schematic of the three exchange regimes. At 0.07 cmc the solution contains monomers, and the isotherm is consistent with small aggregates on the surface. At 0.75 cmc, the solution contains monomers and the isotherm is consistent with micelles at the surface. At 1.5 cmc, the solution contains monomers and micelles, and the micelles have a larger aggregation number.

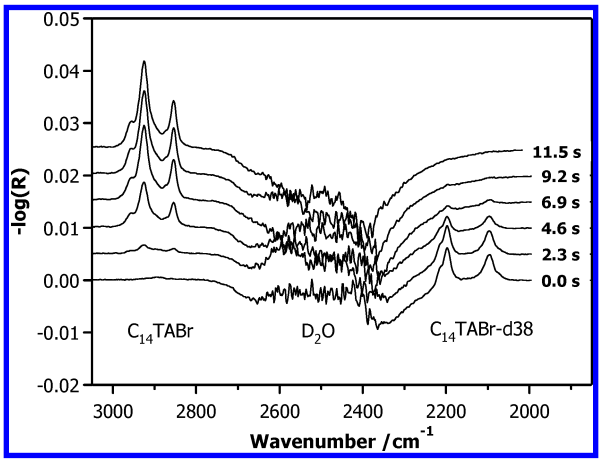

Figure 6. Replacement of $C_{14}TABr$-d_{38} with $C_{14}TABr$ in the evanescent zone. The singal includes a contribution of ~9% from surfactant in bulk. These spectra are referenced to a pure D_2O background. Note the desorption of D_2O from the initial adsorption of $C_{14}TABr$.

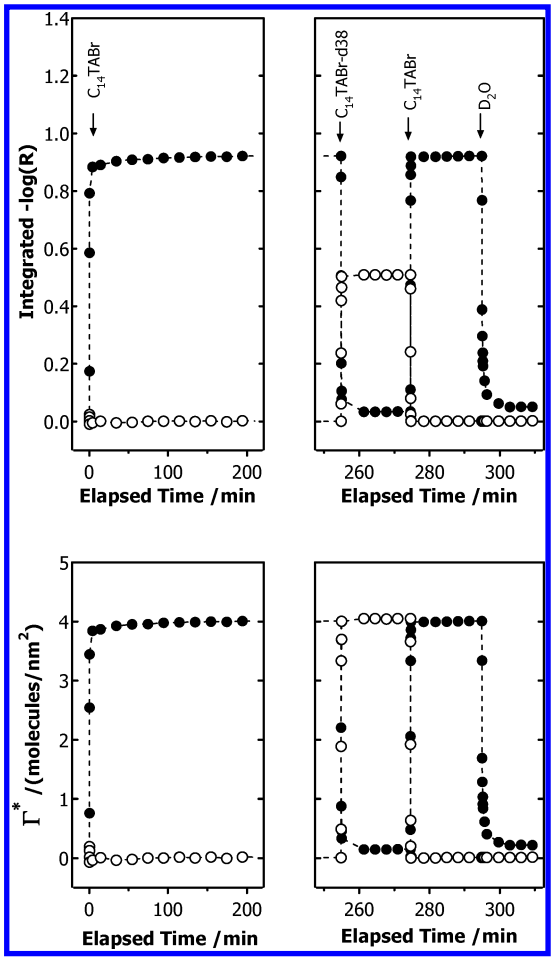

Figure 7. Overview of typical kinetics experiment showing integrated $-\log(R)$ and surface excess for $C_{14}TABr$ (●) and $C_{14}TABr$-d_{38} (○). Γ^* is the surface density that is calculated without subtracting the contribution from surfactant in bulk (see eq 2b). The starting state is pure D_2O; the labeled arrows show the time at which a new solution (in D_2O) was introduced to the cell.

surface spectrum. For equilibrium measurements (Figure 3) we were able to subtract off the contribution from the bulk to obtain the Gibbs surface excess using eq 2a. For kinetics experiments, we did not compensate for contribution from bulk surfactant because of uncertainty as to the exact concentration at each moment. These uncorrected surface concentrations were calculated using eq 2b and are labeled by ∗. Neglect of the same correction for equilibrium measurements overestimates surface concentrations by ~9%. Figure 7 shows raw data and surface excess values for a typical experiment.

Note that the equilibrium adsorbed amount of $C_{14}TABr$-d_{38} is approximately the same as the equilibrium adsorbed amount of $C_{14}TABr$. This together with the constant amount of water during $C_{14}TABr$-d_{38}−$C_{14}TABr$ exchange (Figure 6) suggests that $C_{14}TABr$-d_{38} is an approximate mimic of $C_{14}TABr$ when each is in a pure solution. However, equilibrium measurements of adsorption from equimolar solutions of $C_{14}TABr$-d_{38} and C_{14}-TABr (not shown) show that the surface excess of $C_{14}TABr$ is about 1.2 times the surface excess of $C_{14}TABr$-d_{38} at all concentrations. This shows that adsorption of $C_{14}TABr$ is favored in a mixed film, i.e., that there is a difference in energy of the adsorbed monomer depending on whether the neighbors are perhydrogenated or perdeuterated.

Note also that there is residual CH signal remaining after the $C_{14}TABr$-d_{38} solution has been introduced. The amount is about 2.5% of the total $C_{14}TABr$ signal, which is consistent with the manufacturer's stated H contamination in the $C_{14}TABr$-d_{38}. Thus, within the resolution of our experiment, each surfactant is able to completely remove the other surfactant within about 10 s.

Exchange experiments at 1.5 cmc, 0.75 cmc, and 0.07 cmc are shown in Figures 8−10. The principle result is that exchange of D_2O for surfactant or surfactant for surfactant are both very fast, whereas exchange of surfactant for D_2O is quite slow. The fast rate of adsorption (equilibrium within 10 s) is similar to that observed previously by Atkin et al.[5] using reflectometry (~20 s) and casts some doubt on the very slow adsorption rates (minutes to hours) that have been observed in other work. The novel aspect of the current work is our observation of the very rapid exchange of one surfactant molecule for another at the surface. Figures 8−10 show that this exchange is much faster than the final stages of replacing adsorbed surfactant with water.

The rate of exchange of surfactant between the bulk and the surface depends on the rate of transport to the surface, as well as rates of processes in the diffuse double-layer and the Stern layer. To arrange for more rapid delivery of surfactant to the surface, we performed experiments in which a bubble was used to separate the old and new solutions during exchange. The passage of the bubble through the cell swept out more of the old solution and brought faster moving layers of solution closer to the walls than would occur when the liquids were simply exchanged. The transport time to bring new material to the surface is shorter under this condition than for a normal exchange of solution. Experiments with bubbles in 0.07 cmc

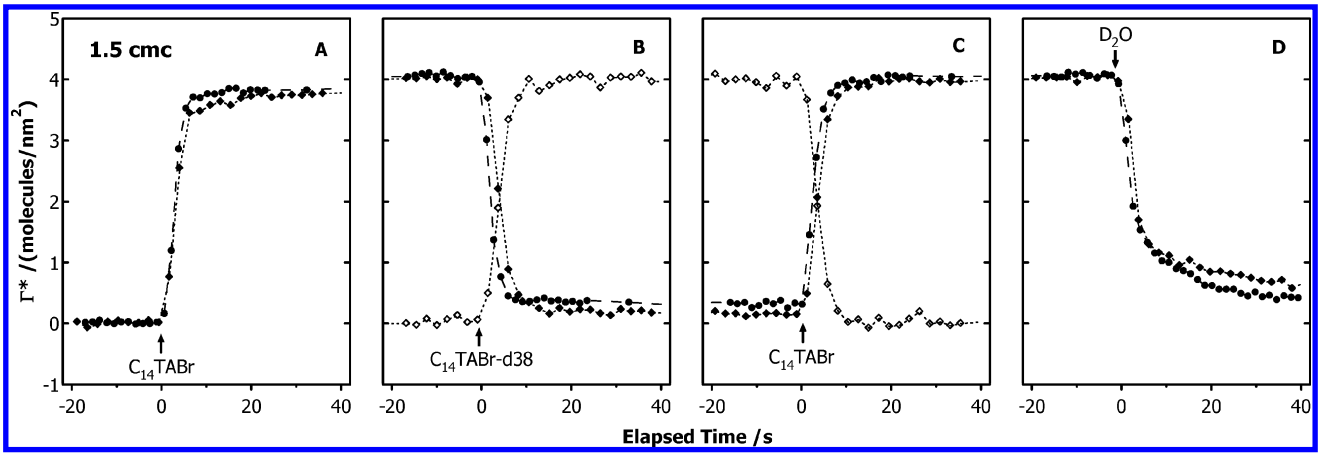

Figure 8. Kinetics of C_{14}TABr exchange at 1.5 cmc and 25.0 °C. Closed symbols show data for C_{14}TABr and open symbols show data for C_{14}TABr-d_{38}. Dashed lines are added to guide the eye. (A) Replacement of D_2O with C_{14}TABr solution. (B) Replacement of C_{14}TABr solution with C_{14}TABr-d_{38} solution. (C) Replacement of C_{14}TABr-d_{38} solution with C_{14}TABr solution. (D) Replacement of C_{14}TABr solution with D_2O. The arrows show the time at which the new solution was introduced to the cell. Separate bubble (●) and no-bubble experiments (♦) are shown on the same graph.

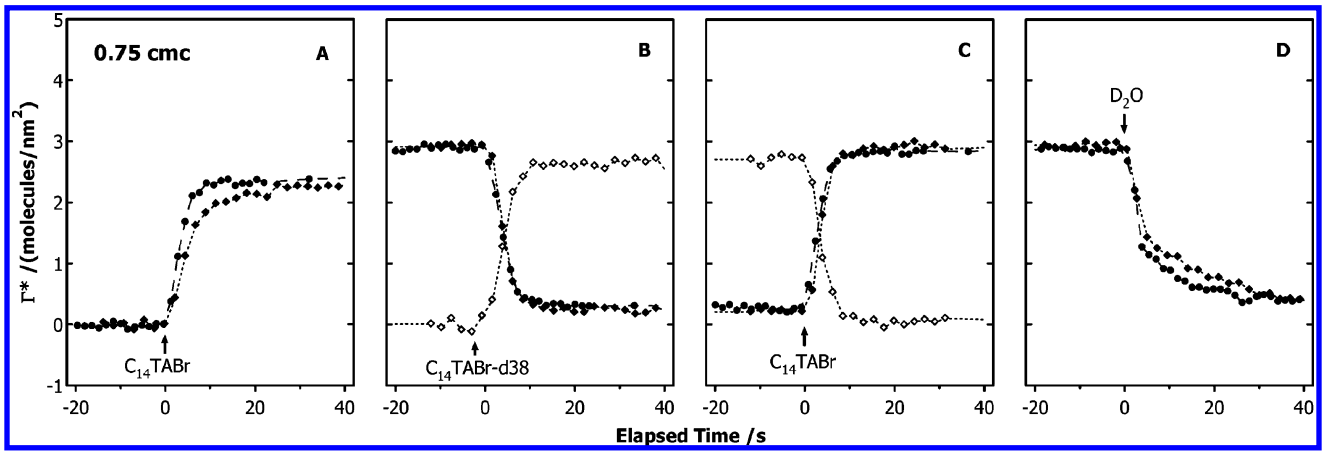

Figure 9. Kinetics of C_{14}TABr exchange at 0.75 cmc and 25.0 °C. Closed symbols show data for C_{14}TABr and open symbols show data for C_{14}TABr-d_{38}. Dashed lines are added to guide the eye. (A) Replacement of D_2O with C_{14}TABr solution. (B) Replacement of C_{14}TABr solution with C_{14}TABr-d_{38} solution. (C) Replacement of C_{14}TABr-d_{38} solution with C_{14}TABr solution. (D) Replacement of C_{14}TABr solution with D_2O. The arrows show the time at which the new solution was introduced to the cell. Separate bubble (●) and no-bubble experiments (♦) are shown on the same graph.

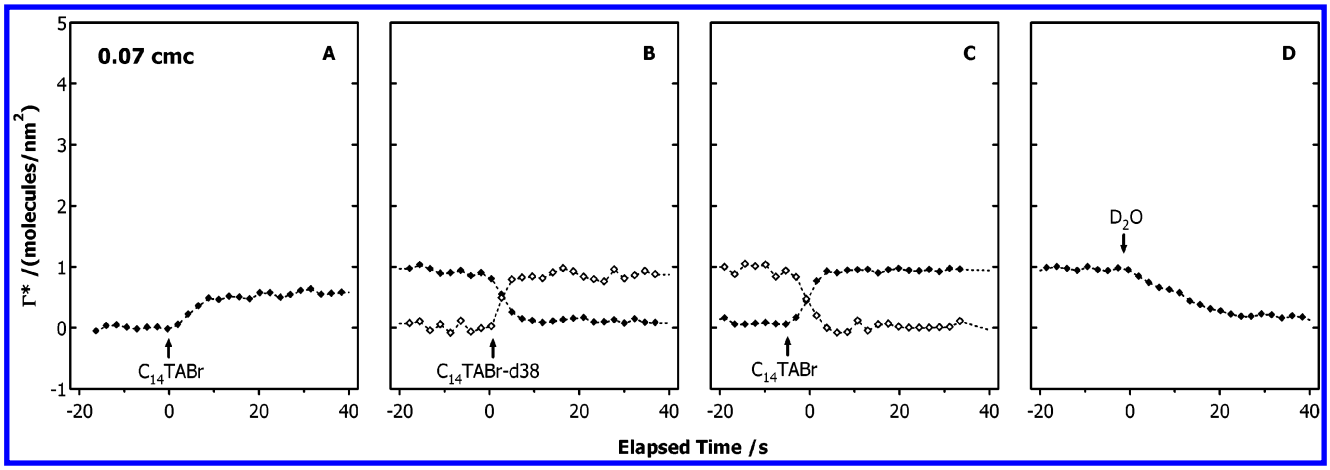

Figure 10. Kinetics of C_{14}TABr exchange at 0.07 cmc and 25.0 °C. Closed symbols show data for C_{14}TABr and open symbols show data for C_{14}TABr-d_{38}. Dashed lines are added to guide the eye. (A) Replacement of D_2O with C_{14}TABr solution. (B) Replacement of C_{14}TABr solution with C_{14}TABr-d_{38} solution. (C) Replacement of C_{14}TABr-d_{38} solution with C_{14}TABr solution. (D) Replacement of C_{14}TABr solution with D_2O. The arrows show the time at which the new solution was introduced to the cell. No bubbles were used in the experiments.

caused a large decrease in the water signal, which made baselining of the methylene stretch difficult, and left us suspicious that the bubble may have touched the reflection element. This is consistent with a tails-out surfactant conformation as shown in Figure 5. Therefore we do not report any bubble experiments for 0.07 cmc.

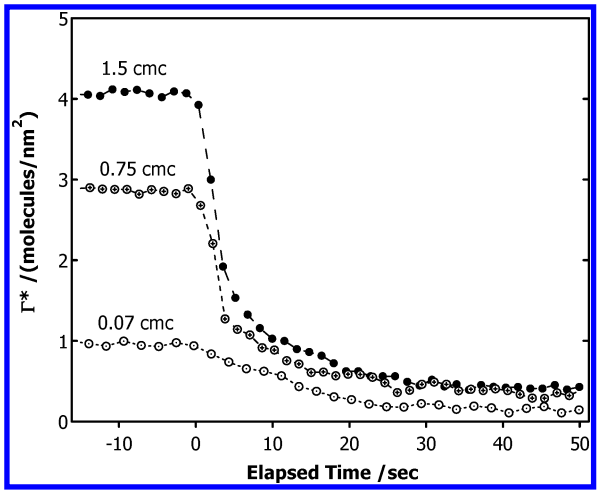

Figure 11. Desorption of $C_{14}TABr$ by pure D_2O at 25.0 °C at three surface excess values, 1.5 cmc (●), 0.75 cmc (⊕), and 0.07 cmc (○). Lines are a guide to the eye.

The bubble experiments demonstrate a faster rate of all exchange processes, thereby showing that the rate of adsorption in our no-bubble experiments is limited by transport processes.

The adsorption rates at different concentrations have been examined by Atkin et al.[5] They observe a concentration region just below the cmc where the adsorption is much slower than at both higher and lower concentrations. At 0.75 cmc, we observe that most of the adsorption occurs in a short period of time, but that a small amount of additional adsorption did occur over a long period of time (observe the break between A and B in Figure 9). The magnitude and form of this additional adsorption was variable in our experiments and will not be considered further here. Neglecting this complication, we find that the time to reach at least 80% adsorption is similar at 0.07 cmc, 0.75 cmc and 1.5 cmc, so we are not able to resolve any special role for micelles in speeding adsorption. Likewise, we measure the same time period to exchange one surfactant for another over a wide range of bulk and surface concentrations. Again, we see no special role for micelles in altering the kinetics of exchange but leave open the possibility that such an effect might be resolved if a way is found to produce a more rapid perturbation from equilibrium.

The desorption of surfactant is slower than the adsorption or the exchange, which allows us to resolve the desorption profile; the relevant data from Figures 8−10 is replotted in Figure 11. At 1.5 cmc a two-stage adsorption is observed: the first 50−60% of the surfactant is removed very quickly and the remaining ~1.2 molecules/nm^2 desorbs at a slower time rate. Starting from a lower concentration (0.75 cmc or 0.07 cmc) produces the same result, a rapid loss of surfactant in the first few seconds followed by a slower loss of the remaining ~1.2 molecules/nm^2. These two rates imply that the there are two environments for the surfactant: a strongly bound and a more weakly bound state. A reasonable hypothesis is that the weakly bound state consists of those molecules held by hydrophobic association of the alkyl chains, and that the strongly bound state is those molecules held to the silica by electrostatic forces. The surface density at which the strongly bound material is found in a desorption experiment is greater than the surface density at the top of the sudden rise in the adsorption isotherm (~0.8 molecules/nm^2). This is not completely surprising, it merely suggests that the addition of extra surfactant causes more surfactant to bind electrostatically (by displacing protons from the surface.) There is ample evidence for charge regulation by quaternary ammonium surfactants on silica.[39,40]

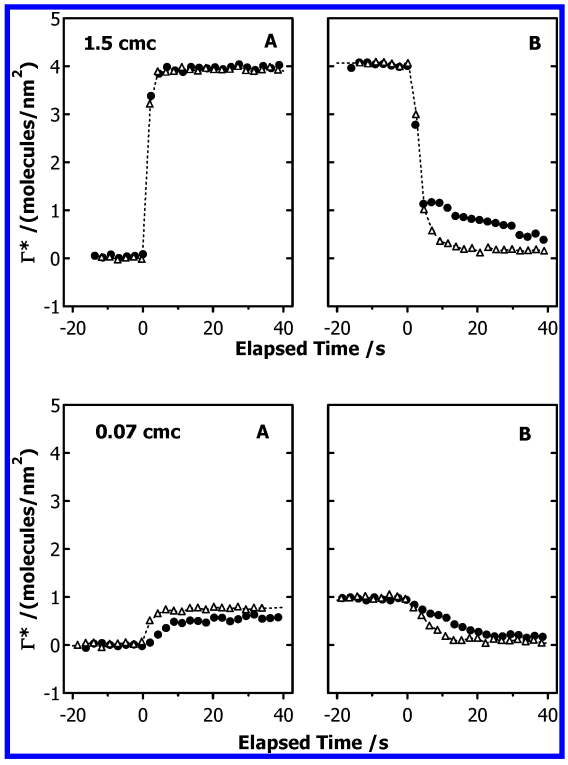

Figure 12. Influence of KBr on the adsorption and desorption of $C_{14}TABr$ from silica surface at 25.0 °C. Dashed lines are a guide to the eye. (A) The circulating solution was changed from D_2O to $C_{14}TABr$ (circles), and from an equimolar KBr solution to $C_{14}TABr$ (triangles). (B) Desorption of surfactant by D_2O (circles), and KBr solutions (triangles). The surfactant was allowed to equilibrate for 3.5 h prior to desorption.

We also monitored the frequency of maximum absorption during the desorption process. Figure 4 shows that the frequency simply slides back though the same frequencies as observed during the equilibrium adsorption experiment. One might expect that if whole micelles were desorbing, the amount adsorbed would drop while the frequency would remain the same, but this does not happen. The data are consistent with the loss of monomers from all micelles to give a succession of smaller aggregation numbers during desorption.

It is interesting that the exchange of surfactant for water is so much slower than the exchange of surfactant for another surfactant molecule (In Figures 8 and 9, compare B or C to D.) After the first part of the adsorbed micelle has desorbed, the remaining adsorbed aggregate passes through an aggregation number or state that experiences a big barrier to further desorption. Thus exchange of surfactant for water at the surface is analogous to the slow relaxation in bulk micelles (τ_2) whereas exchange of one monomer for another at the surface is analogous to τ_1. The disintegration of a bulk micelle is hindered by aggregation states that have large exposure of hydrocarbon to water. The disintegration of a surface micelle is similarly hindered, but when the surfactant and surface are oppositely charged, there should also be an electrostatic barrier to desorbing some monomers.

To examine the electrostatic component of the activation barrier to desorption, we also measured the desorption into a salt (KBr) solution. To facilitate comparison to results for exchange with $C_{14}TABr$-d_{38}, we used the same concentration of salt as surfactant. Figure 12 shows that the rate of the second (slow) portion of desorption is much greater in salt solution and is similar to the rate in $C_{14}TABr$-d_{38}. This supports the hypothesis that an electrostatic force is important in the rate-

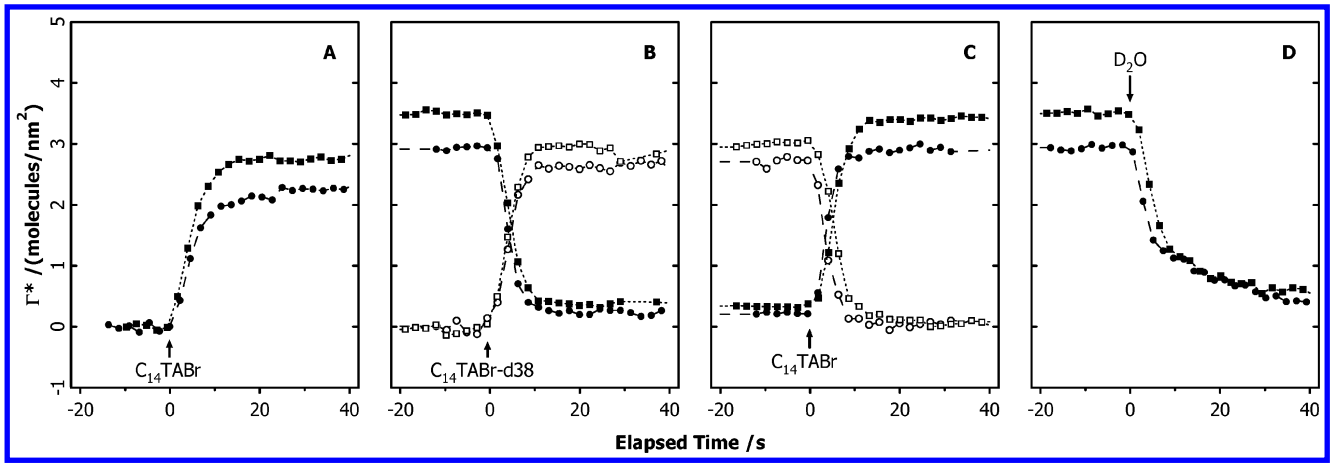

Figure 13. Effect of temperature on the kinetics of $C_{14}TABr$ exchange at 0.75 cmc. Data at 25.0 ± 0.1 °C are represented by circles and data at 6.0 ± 0.3 °C are represented by squares; closed symbols show data for $C_{14}TABr$ and open symbols show data $C_{14}TABr$-d_{38}. Dashed lines are added to guide the eye. (A) Replacement of D_2O with $C_{14}TABr$ solution. (B) Replacement of $C_{14}TABr$ solution with $C_{14}TABr$-d_{38} solution. (C) Replacement of $C_{14}TABr$-d_{38} solution with $C_{14}TABr$ solution. (D) Desorption of $C_{14}TABr$ using D_2O. The arrows show the time at which the new solution was introduced to the cell. No bubbles were used in the experiments.

determining step during desorption. If this electrostatic attachment to the solid could be removed entirely, one might expect desorption to be limited only by the existence of (unfavorable) aggregation states with exposed hydrocarbon, and therefore to have a time constant similar to τ_2 measured for bulk micelles.

Silica is negatively charged in water and is made positive by adsorption of surfactant; so desorption below the point of zero charge occurs against an electrical potential. Adsorption of K^+ ions in the salt (exchange of K^+ for $C_{14}TA^+$) should reduce the electrostatic barrier by reducing the surface potential and the Debye length. In a pure D_2O or H_2O solution, the only cations available to prevent the build up of a negative potential are the very dilute deuterons or protons.

The rate of adsorption also shows a rapid adsorption followed by a slower adsorption. Working on the hypothesis that the slow approach to equilibrium resulted from a slow surface rearrangement involving hydrogen, we *pretreated* the silica surface with KBr solution to remove hydrogen, then displaced the KBr solution with surfactant solution. (Because our experiments are in D_2O solvent, we expect that nearly all the dissociable surface protons have been replaced with deuterons.) In this experiment, we are attempting to displace D^+ with K^+ before the surfactant in present, but we have no K^+ present in solution after the exchange. This removes the possible rate enhancing effect of long-range electrostatic screening on the rate of surfactant adsorption. At 0.07 cmc we see a distinctly faster adsorption when the surface is pretreated with K^+, which is consistent with the hypothesis of D^+ desorption being the limiting step. Above the cmc, we see no change (the rate is already at our resolution), and the results at 0.7 cmc were too variable to reach a conclusion.

We also monitored the surfactant exchange processes at 6.3 °C and 0.75 cmc. This is about 1 °C above the freezing point of D_2O and about 8 °C below the Krafft temperature of $C_{14}TABr$. (We measured the Krafft temperature in D_2O at 14 °C.) Some earlier studies of surfactant adsorption and desorption that reported slow rates were performed on surfactants near the Krafft temperature (e.g., $C_{16}TABr$ at 20−25 °C) and we were curious to see whether perhaps slow adsorption/desorption rates correlated with an experimental temperature below the Krafft temperature.

Figure 13 shows that the kinetics of $C_{14}TABr$ exchange below the Krafft temperature are similar to the kinetics above the Krafft temperature. There is very little change in adsorption or surfactant−surfactant exchange rates. The asymmetric CH stretch mode peak is located at 2924.4 cm^{-1} for the 6.0 °C experiment and at 2925.2 cm^{-1} for the same experiment at 25.0 °C, which suggests a slightly more crystalline adsorbed state at 6.0 °C. However, the similarity of the rates at 6.0 and 25.0 °C shows the absence of a significant effect due to surface freezing. We are able to resolve a large increase in surface excess for the lower temperature, which is perhaps related to a decrease in solubility of surfactant in bulk solution.

AFM Experiments. The slow rate of perturbation from equilibrium that was available by changing the concentration in the ATR−IR experiments led us to examine a faster way of perturbing the adsorbed structure. We performed AFM experiments in which we measured the frequency dependence of the force required to displace a layer of surfactant at 1.5 cmc from the surface of silica. (The adsorbed surfactant forms a barrier to approach of the AFM tip.) In this case, we apply a mechanical force to displace the surfactant rather than the chemical force (dilution) used in the ATR−IR experiments. Our analysis of these measurements assumes that, for successive oscillations, there is a large overlap of the strike zone of the tip on the sample. The typical lateral drift in our measurement in about 0.1 nm s^{-1}. The average lateral displacement of the tip between striking the sample depends on the frequency, and in our experiments, the lateral drift between strikes is in the range 0.1−0.01 nm. This is a small fraction of the tip width (>10 nm), so the tip does mainly strike the same region on consecutive oscillations.

The value of comparison to AFM experiments of this type is diminished because we do not know the mechanism of displacement of surfactant by the AFM tip. Because the load is not homogeneous across the surface, the surfactant could be displaced into solution (as in the ATR−IR experiments) or pushed across the interface. Also, because the zero of separation between the tip and sample is not known, the results may be showing displacement of only part of the surfactant film.

The results are shown in Figure 14. Even at repeat approach rates as high as 56 Hz, the surfactant is able to reassemble on the surface between tip approaches, suggesting an exchange rate at least 50 times faster than measured in our ATR−IR experiments. At 112 Hz, the barrier height is similar but the thickness of the surfactant layer is much smaller than at lower

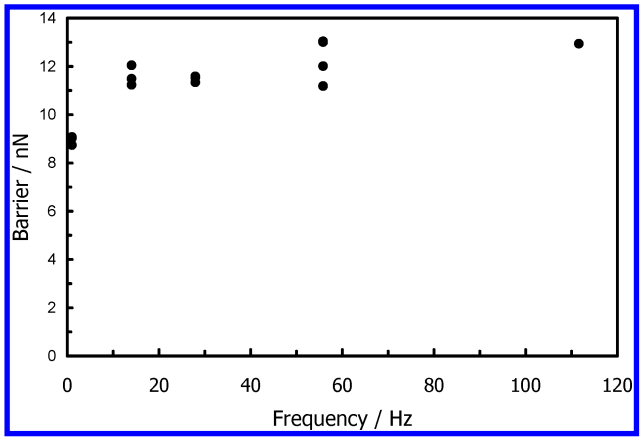

Figure 14. Effect of the frequency of approach on the maximum force barrier experienced by an AFM tip on approach to a surface film of C_{14}TAB adsorbed to a silicon wafer. At all frequencies except 112 Hz, the tip jumped about 4 nm toward the silicon wafer at the maximum in force. The AFM tip may also be coated in surfactant.

frequencies, suggesting that the full surfactant film is not able to recover at 112 Hz. The small increase in height between 1 and 14 Hz shows that there is also an adsorption relaxation process in this frequency range.

Modeling of Monomer Exchange Kinetics

Our experiments that facilitate solution exchange with bubbles show that surfactant exchange is transport limited in the absence of bubbles: faster exchange is observed when the bubble is used to decrease the thickness of the stagnant layer near the surface. Despite this limitation, the observed rates of exchange of deuterated for protonated surfactant are quite fast, and it is interesting to compare the observed rate to the known rate in solution. The desorption rate for a single C_{14}TABr monomer in a bulk micelle is 10^4 s^{-1}. This value was determined by Gharibi et al.[7] on the basis of monomer concentration corrections to the work of Kato et al.[41]

Because we know that our results are diffusion limited, there is little point in making a detailed model of the desorption; we can only determine a lower bound to the rate. Here we assume that only the monomers in the solution side of the micelle can leave; the remainder are prevented or at least hindered from departing by the solid surface. However, we assume that exchange between positions in the micelle is very rapid, so that monomers on the solid side can translate around the micelle and then exchange with solution monomers. Furthermore, we assume that the rate of exchange is determined by the desorption rather than the adsorption (in keeping with an activated desorption as described by Aniasson et al.), and that the rate constant for protonated monomer desorption is simply proportional to the number of monomers remaining in the micelle (i.e., the activation for desorption is independent of whether the neighbors are protonated or deuterated). Thus we arrive at a simplified kinetic scheme as follows:

$$H_{N-x}D_x \rightleftharpoons H_{N-x-1}D_x + H \qquad k = k'(N-x)/2$$

where H represents C_{14}TABr, D represents C_{14}TABr-d_{38}, and k' is the rate of desorption for an individual monomer in the micelle. (In Annianson et al.'s nomenclature, $k' = k/N$). The factor of $^1/_2$ is simply a rough guess as to the fraction of monomers that can leave from a micelle.

Values of N for C_{14}TABr at the silica−water interface were measured by Ström et al.[38] They are 53, 72, 115, and 143 for concentrations of 1, 2, 3, and 3.1 mM, respectively. The 100 or so simultaneous equations for aggregates of different composition were solved using Matlab, and the overall desorption of H was fitted to our measured desorption. In fact, the overall rate is relatively insensitive to the aggregation number in the range $N = 70-200$. The fitted value of k' was 1 s^{-1}. Thus, the lower bound for the rate of desorption of an individual monomer is 1 s^{-1}, and so the monomer desorption from these adsorbed micelles is no more than 10^4 times slower than from bulk micelles.

Conclusions

Good agreement between adsorption isotherms measured by ellipsometry and by ATR−IR lend further support to the idea that ATR−IR is a valid technique for measuring the amount of adsorption to a solid−liquid interface. ATR−IR has an additional advantage over ellipsometry in that it can also be used to simultaneously measure the kinetics of exchange and equilibrium adsorption of two species individually and simultaneously (if they have distinct chromophores). We have used this capability to show that hydrogenated surfactant adsorbs to a greater extent than deuterated surfactant from 1:1 mixtures, but the amount of adsorption and the amount of water in the film is the same at a variety of concentrations when each surfactant is adsorbed separately.

We have also shown that the rate of exchange of C_{14}TABr between aqueous solution and the aqueous−silica interface is very rapid: even under conditions where delivery of the new adsorbate to the interface is limited by transport to the surface, complete exchange in our apparatus occurs within 10 s. This corresponds to a fitted rate constant for desorption of >1 s^{-1}. Thus, the rate of monomer desorption from the surface is no more than 10^4 times slower than the rate of desorption from a bulk micelle. AFM experiments on a faster time scale suggest that surfactant adsorption may even be an additional 500 times faster than measured by ATR−IR. Clearly, a new and faster method for changing the surface state is required to further reduce the uncertainty in the exchange rates.

The rapid exchange of surfactant at the solid−liquid interface has implications for the use of surfactants in controlling colloidal stability. The fast exchange means that the surface excess of surfactant on colloidal particles is not necessarily constant during colloidal collisions and supports the idea that changes in adsorption during collisions (proximal adsorption)[42] should be considered in theories of colloidal stability.

Adsorption of surfactant from solution (exchange with solvent and or simple cations) is also a fast process, which in dilute surfactant solutions can be accelerated by pretreating the surface with salt. This suggests that desorption of hydrogen ions from the silica surface is a rate limiting step in adsorption of the cationic surfactant from a dilute surfactant-only solution.

Desorption of surfactant into pure D_2O is also a rapid process, but sufficiently slow compared to diffusion that we are able to resolve some structure in the desorption−time profile. Above the cmc, the first two-thirds of the surfactant desorbs very quickly, and the remainder desorbs slowly. This slow-desorbing fraction is slightly greater in amount than the first plateau in the adsorption isotherm. Exchange of surfactant with salt solution shows that this slow-desorbing fraction is held by electrostatic interactions. Our results support the conclusion that desorption of ionic surfactant from a charged surface occurs in two stages: rapid loss of surfactant that is held by hydrophobic interactions and slower loss of surfactant that is held by electrostatic interactions with the surface.

The kinetics of adsorption, desorption, and exchange at 6.3 °C (1 °C above the freezing point of the solvent and 8 °C below the Krafft temperature) is almost the same as at 25.0 °C. There is no indication of a slowing of exchange associated with surface freezing. However, the density of adsorption is greater, and there is a shift of the IR peak maximum to lower frequency at 6.3 °C, which shows that the surfactant finds itself in a slightly different state on the surface at the lower temperature.

More rapid exchange is made possible by passing a bubble through the ATR cell between solutions thereby allowing access to slightly faster processes. Attenuation of the solvent absorption peak provides a warning when the bubble passes close to the silica−water interface.

Acknowledgment. We thank Professor Tom Ward for extended use of his infrared spectrophotometer, Professor Mark Anderson for use of his ATR accessory and wire grid polarizers, and Professor Brian Vick for help with the Matlab program. This work is based on research supported by the National Science Foundation Grants 0203987 and 0216129.

References and Notes

(1) Tiberg, F.; Jönsson, B.; Lindman, B. *Langmuir* **1994**, *10*, 3714−3722.
(2) Pagac, E. S.; Prieve, D. C.; Tilton, R. D. *Langmuir* **1998**, *14*, 2333−2342.
(3) Neivandt, D. J.; Gee, M. L.; Hair, M. L.; Tripp, C. P. *J. Phys. Chem. B* **1998**, *102*, 5107−5114.
(4) Biswas, S. C.; Chattoraj, D. K. *J. Colloid Interface Sci.* **1998**, *205*, 12−20.
(5) Atkin, R.; Craig, V. S. J.; Biggs, S. *Langmuir* **2001**, *17*, 6155−6163.
(6) Aniansson, E. A. G.; Wall, S. N.; Almgren, M.; Hoffman, H.; Kielmann, I.; Ulbricht, W.; Zana, R.; Lang, J.; Tondre, C. *J. Phys. Chem.* **1976**, *80*, 905−922.
(7) Gharibi, H.; Takisawa, N.; Brown, P.; Thomason, M. A.; Painter, D. M.; Bloor, D. M.; Hall, D. G.; Wyn-Jones, E. *J. Chem. Soc., Faraday Trans.* **1991**, *87*, 707−710.
(8) Gulari, E.; Couzis, A. *Langmuir* **1993**, *9*, 3414−3421.
(9) Manne, S.; Gaub, H. E. *Science* **1995**, *270*, 1480−1482.
(10) Subramanian, V.; Ducker, W. A. *Langmuir* **2000**, *16*, 4447−4454.
(11) Couzis, A.; Gulari, E. *Langmuir* **1993**, *9*, 3414−3421.
(12) Jang, W. H.; Miller, J. D. *Langmuir* **1993**, *9*, 3159−3165.
(13) Sperline, R. P.; Song, Y.; Freiser, H. *Langmuir* **1992**, *9*, 2183−2189.
(14) Singh, P. K.; Adler, J. J.; Rabinovich, Y. I.; Moudgil, B. M. *Langmuir* **2001**, *17*, 468−473.
(15) Dobson, K. D.; Roddick-Lanzilotta, A. D.; McQuillan, A. J. *Vibr. Spectrosc.* **2000**, *24*, 287−295.
(16) Sukhishvili, S. A.; Granick, S. *J. Phys. Chem. B* **1999**, *103*, 472−479.
(17) Sperline, R. P.; Muralidharan, S.; Freiser, H. *Langmuir* **1986**, *3*, 198−202.
(18) Patist, A.; Kanicky, J. R.; Shukla, P. K.; Shah, D. O. *J. Phys. Chem. B* **2002**, *245*, 1−15.
(19) Sperline, R. P.; Song, Y. *Langmuir* **1997**, *13*, 6985−6994.
(20) Hoffmann, H.; Mayer, U.; Brunner, H.; Kattner, J.; Vallant, T. *Langmuir* **1999**, *15*, 5339−5346.
(21) Sperline, R. P. *Langmuir* **1997**, *13*, 3715−3726.
(22) Sperline, R. P.; Song, Y.; Freiser, H. *Langmuir* **1997**, *13*, 3727−3732.
(23) Kung, K.-H. S.; Hayes, K. F. *Langmuir* **1993**, *9*, 263−267.
(24) Ninness, B. J.; Bousfield, D. W.; Tripp, C. P. *Colloids Surf. A* **2002**, *203*, 21−36.
(25) Hansen, W. N.; Kuwana, T.; Osteryoung, R. A. *Anal. Chem.* **1966**, *38*, 1810−1821.
(26) Sperline, R. P.; Jeon, J. S.; Raghavan, S. *Appl. Spectrosc.* **1992**, *46*, 1644−1648.
(27) Sperline, R. P.; Freiser, H. *Langmuir* **1990**, *6*, 344−347.
(28) Thompkins, H. G. *Appl. Spectrosc.* **1974**, *28*, 335−341.
(29) Sperline, R. P.; Song, Y.; Freiser, H. *Langmuir* **1994**, *10*, 37−44.
(30) Sperline, R. P. *Appl. Spectrosc.* **1991**, *45*, 677−681.
(31) Hansen, W. N. In *Advances in Electrochemistry and Electrochemical Engineering*; Delahay, P., Tobias, C. W., Eds.; John Wiley & Sons: New York, 1973; Vol. 9, pp 1−60.
(32) Hansen, W. N. *J. Opt. Soc. Am.* **1968**, *58*, 380−390.
(33) Citra, M. J.; Axelsen, P. H. *Biophys. J.* **1996**, *71*, 1796−1805.
(34) Picard, F.; Buffeteau, T.; Desbat, B.; Auger, M.; Pezolet, M. *Biophys. J.* **1999**, *76*, 539−551.
(35) Bertie, J. E.; Ahmed, M. K.; Eysel, H. H. *J. Phys. Chem. B* **1989**, *93*, 2210−2218.
(36) Koppaka, V.; Axelsen, P. H. *Langmuir* **2001**, *17*, 6309−6316.
(37) Sperline, R. P.; Muralidharan, S.; Freiser, H. *Appl. Spectrosc.* **1986**, *40*, 1019−1022.
(38) Ström, O.; Hansson, P.; Jönnson, B.; Södermann, O. *Langmuir* **2000**, *16*, 2469−2474.
(39) Goloub, T. P.; Koopal, L. K.; Bijsterbosch, B. H.; Sidorova, M. P. *Langmuir* **1996**, *12*, 3188−3194.
(40) Goloub, T. P.; Koopal, L. K. *Langmuir* **1997**, *13*, 673−681.
(41) Kato, S.; Nomura, H.; Honda, H.; Zielinski, R.; Ikeda, S. *J. Phys. Chem.* **1988**, *92*, 2305−2310.
(42) Subramanian, V.; Ducker, W. A. *J. Phys. Chem. B* **2001**, *105*, 1389−1402.